An experimental study on variation of thermal fields during the deformation of a compressive en echelon fault set*

LIU Peixun**, MA Jin, LIU Liqiang, MA Shengli and CHEN Guoqiang

(Laboratory of Earthquake Dynamics, Institute of Geology, China Earthquake Administration, Beijing 100029, China)

Accepted on September 22, 2006

Abstract The temperature variations during deformation of a compressive en echelon fault set in a rock sample were measured by a surface measurement system with multi-point platinum resistance thermometers and an infrared thermal image system. The measurements obtained by the two systems were in agreement with each other, indicating a relationship between temporal-spatial variations of the thermal field and changes of stress and strain. At varied structural positions of the rock sample, the rising of the temperature was different, implying distinct stress distributions at these positions. In the experiment, the deformation process of the sample included three stages: elastic deformation, stick-slip, and rupture. Correspondingly, the variation process of temperature had also three stages, each of which had its own temperature rising profile. And the thermal radiation field showed a similar process. These phenomena mean that the dominant mechanisms of temperature rising in all stages of deformation are different. Experimental results provide a physical basis for the study of current fault activities by using data of satellite infrared images.

Keywords: en echelon fault set, stick-slip, thermal infrared radiation, temperature, mechanism of temperature rising.

Studies of faulting using NOAA satellite infrared image data have shown that variations of infrared images contain information associated with current activities of faults, some of which are closely related to changes of regional stress and strain fields[1]. Images of satellites are, however, influenced by variations of many kinds of factors, including stress and strain as well as changes of mass state, like involvement of water and gas[2,3]. Therefore satellite images are integrated results, from which the information on the stress related to faulting is hard to get.

Physically, mechanical deformation of rock can cause temperature variations[4,5]. When a rock sample experiences a deformation, such as elastic deformation, plastic deformation, rupture, or frictional slip, the intensity of stress at varied positions in the sample should be different. Now the questions are whether these differences can be recognized from changes of the thermal field, what effect on infrared radiation will be produced by changes of deformation mechanisms, and how to identify the variations of instability of the fault and the sudden stress drop in a rock sample on the thermal images.

Physical modeling in laboratories is one of possible approaches to address these issues. Because in laboratories temperature and other conditions of rock deformation can be artificially controlled and mass state is usually known, so that we can design various schemes of experiments to measure thermal variations during faulting of samples. Based on these observations, we can study further the mechanisms of temperature rising associated with faulting, and interpret information from satellite images. This paper presents our experimental results of variation of thermal fields during the deformation of an en echelon faults.

1 Experimental conditions and apparatuses

In the experiment, we used a thermal imaging system and platinum resistance contact-type thermometers to simultaneously measure temperature variations caused by rock deformation. Meanwhile stress and displacement were also measured.

The thermal imaging system was an IR913A type apparatus produced by the Gaode Corporation, Wuhan, China. It has the following technical parameters: spectrum range was 8—14 μm, temperature range 10—350℃, mode transform 16 bit, temperature resolution 0.06 K, focal length of lens 40 mm, focusing range 0.5—∞ m, and spatial resolution 320

* Supported by National Natural Science Foundation of China (Grant Nos: 90202018 and 40572125), National Program on Key Basic Research Projects (2004CB418405), and Special Founds from China Earthquake Administration

** To whom correspondence should be addressed. E-mail: liupeixun@sina.com

$\times$ 240 pixels[6]. By adding an 1394 interface, this system can perform continuous data transmission and recording with the largest recording time merely depending on the room of the disk and the fastest recording rate of 50 pictures per second. In this experiment, the distance between the thermal imaging system and the sample was 0.65 m and the thermal image sampling was 12.5 pictures per second. Before and after the experiment, thermal image sections at uniform temperature were recorded respectively to serve the background field correction for data processing.

Since the employed thermal imaging system is of the non-refrigeration type, long-time recording has serious zero drift and distortion of the background field. Hence, corrections were made by using the recorded uniform temperatures before and after the experiment. In addition, low-pass filtering was performed to overcome the problem of strong noise at high frequencies in the thermal infrared thermal image data. As the thermal imaging apparatus used in this test has a large deviation of temperature its calibration needs to be solved, here we concern only the relative variations of the measured brightness temperature of thermal radiation (T_B) instead of accurate values of temperature changes.

Meanwhile, we also used a set of platinum resistance thermometers to measure temperatures of the sample in a synchronous manner with the thermal imaging system. These thermometers have the following parameters: temperature measurement range -10—60℃, temperature resolution 2 mK, and sampling rate 5 Hz. The sensitivity of these thermometers is one magnitude higher than that of the thermal imaging system, so it can serve as the calibration standard for the thermal imaging system. By rapid scans over many points on the sample, these thermometers can obtain spatial distribution patterns and temporal evolution processes of the temperature field on the sample, which can be compared with the infrared images for analysis.

During the experiment, a thermo-hygrograph and an infrared thermometer were used to monitor the environment of the laboratory. And many measures were taken to suppress infrared background noise and disturbance[6]. The actual temperature and humidity of the environment in the laboratory were 24.8℃ and 0.75, respectively.

The sample was made by granodiorite from the Fangshan District, Beijing with a size of 500 mm $\times$ 300 mm $\times$ 50 mm. On the sample a slot-cutting was made at an angle of 31° to Y axis and filled with gypsum. The structure of the sample is shown in Fig. 1, in which blue circles are positions of thermometers, and the area drawn by dashed rectangle is the target of thermal image analysis.

Considering many experimental results concerning physical field evolution of en echelon samples in our laboratory, we did not use other types of detectors to measure strain, displacement in order to avoid interference on thermal field measurement by these exothermic gauges[7—10].

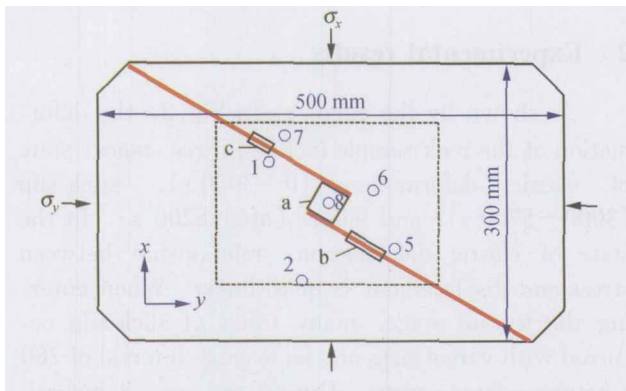

Fig. 1. Structure of the sample and positions of thermometers and studied area of thermal image. Red lines denote faults, blue circles with numerals are measured points on the specimen where thermometers were fixed. Dashed rectangular area is the studied area of thermal radiation, where slats a, b and c indicate the studied area of brightness temperature curves in Fig. 5.

The two-direction servo-control system was used to apply load on the sample. During the experiment, the load in both directions was forced to 5 MPa and maintained constant (5 MPa) in the X direction, then the load in the Y direction was applied by displacement rate of 0.5 μm/s. Fig. 2 shows the varia-

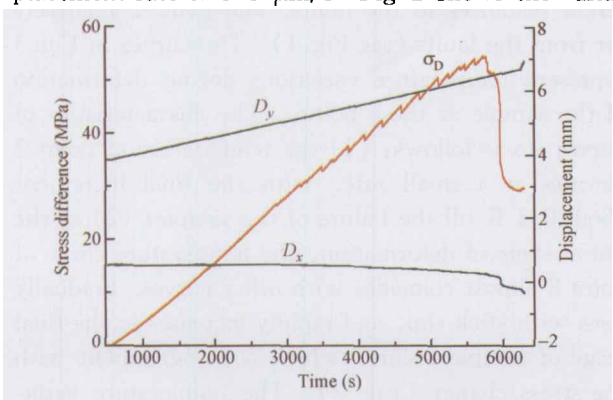

Fig. 2. Process of differential stress σ_D and displacement in X and Y directions. Red line indicates differential stress σ_D, D_X and D_Y represent the displacement in X and Y directions, respectively.

tion of stress and displacement in both directions with time, where the curves D_X and D_Y represent the displacement in X and Y directions versus time, D_Y keeps the displacement rate of 0.5 μm/s until 6000 s. And the σ_D curve shows differential stress with time, where $\sigma_D = \sigma_Y - \sigma_X$.

Compared with previous work done by others[11—24], this experiment was performed by the strictly controlled temperature and humidity in the laboratory, and characterized by the synchronous measurement of temperature variation with time by two independent tools, and continuous transmission of thermal imaging data with improved temporal resolution.

2 Experimental results

As shown by the curve σ_D in Fig. 2, the deformation of the rock sample includes three stages: state of elastic deformation (0—3000 s), stick-slip (3000—5700 s), and failure (after 5200 s). In the state of elastic deformation, relationship between stress and displacement is quasi-linear. When entering the second stage, many times of slick-slip occurred with varied sizes and an average interval of 280 s between large events. During the test, temporal-spatial variations of thermal images on the sample in these stages of deformation were observed.

2.1 Temperature elevation versus positions with respect to the faults

Temperature variation with time was measured at some points on the sample (Fig. 3) by the platinum resistance thermometers, where point 8 located within jog area, point 6 near the ends of the faults, points 1, 5, and 7 on the both sides of the faults with different distances to the faults, and point 2 relatively far from the faults (see Fig. 1). The curves in Fig. 3 represent temperature variations during deformation of the sample at these points. The characteristics of curves are as follows: (1) the temperature at point 2 elevates at a small rate, with the final increment about 0.1 K till the failure of the sample; (2) at the initial stage of deformation, the temperature curve of point 8 almost coincides with other curves, gradually rises with stick-slip, and rapidly increases in the final stage of sample failure, which is in agreement with the stress change (Fig. 2). The temperature variations at point 6, which is close to the ends of the faults, are getting remarkable during the rupture of the jog area; (3) variation of temperature at points 1, 5 and 7 is different and depends on the distance from fault; (4) it was observed that rapid temperature elevation and stress drop occurred synchronously at the points in the jog area and near the faults during the stick-slip event, while such responses did not happen at the point far from the faults. It implies that variations of temperatures are closely associated with the stress state of varied positions on the sample.

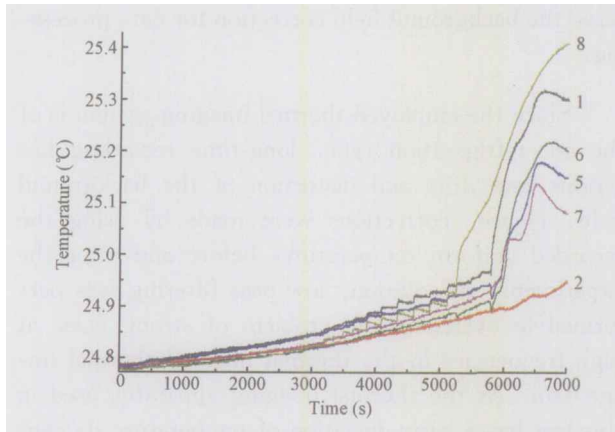

Fig. 3. Temperature variations with time at measurement points. Numerals on the curves represent point positions as shown in Fig. 1.

2.2 Temperature rising rates versus deformation stages

Curves in Fig. 3 shows not only temperature variation versus positions, but also temperature rising rate at measurement points on the sample in different deformation stages. Table 1 lists these varied average rates of temperature elevation for each deformation stage.

Table 1. Average temperature rising rate at measurement points on the sample in each deformation stage (unit: mK/s)

Point	Elastic deformation	Stick-slip	Failure
2	0.011	0.024	0.042
6	0.013	0.031	0.177
7	0.015	0.034	0.101
8	0.016	0.041	0.274
5	0.02	0.035	0.129
1	0.02	0.042	0.204

In the elastic deformation stage (0—3000 s), temperature was raised with differential stress. The least growth rate (0.01 mK/s) appeared at point 2 and the largest rate (0.02 mK/s) appeared at points 1 and 5. In conjunction with the curve σ_D of stress versus time (Fig. 2), the temperature growth rate

with stress was calculated to be 1.2 mK/MPa on average.

In the stick-slip stage (3000—5000 s), the temperature rising rate was much larger than the first stage. The temperatures near the faults elevated with time in a step-like manner, where the temperatures rose suddenly when stick-slip occurred, and maintained constant or declined slowly between stick-slip events. At the points distant from the faults, the relationship between temperature elevation and stick-slip was not conspicuous. For this stage the lowest temperature elevation rate was 0.02 mK/s at point 2 and the highest one was 0.04 mK/s at points 1 and 8. The average temperature increasing rate with stress was 3—4 mK/MPa.

The third deformation stage, i. e. the failure stage of the sample was characterized by high rates of temperature elevation, even including the points distant from the faults. At point 2 appeared the smallest rate of 0.04 mK/s and the largest rate 0.2—3 mK/s was observed at points 8 and 1.

2.3 Stick-slip and temperature variations

We observed that different temperature variations occurred at measurement positions on the tested specimen in response to stick-slip events of the faults. For instance, the temperatures at points 1 and 5 elevated greatly, and that at point 7 increased by a relatively small amplitude during stick-slip event (Fig. 4, Table 2). As shown in Figs. 1 and 4, points 1 and 5 lie in areas with high stress and point 7 is in an area of low stress. Point 8 in the jog area exhibits a distinct feature, where the temperature grows rapidly with stick-slip events. Physically, each stick-slip event along the faults can cause stress increase at the site which is the reason for the temperature elevation. The temperature rising becomes obvious after 3858 s. It may be resulted from the failure in the jog area and heating by frictional sliding.

Table 2. Rising rate and declining rate of temperature before and after stick-slip event at 3849 s (unit: mK/s)

Point number	Rising rate	Declining rate
8	0.906	−0.045
1	0.296	0
5	0.283	−0.011
7	0.074	0

2.4 Stick-slip and thermal image variation

In the experiment, we focused on the thermal images of the central portion of the sample. From these images, we calculated variation of average values T_B(brightness temperature of thermal radiation) in the jog area (rectangle a in Fig. 1) and left and right faults (rectangles b and c in Fig. 1) on the sample (Fig. 5). It was a general trend that values of T_B increased with the stick-slip process on the faults. Every stick-slip event was followed by a rapid elevation of T_B which was equivalent to temperature rising. In the jog area a rapid elevation of T_B followed a stick-slip and then the T_B declined gradually. Different from this case, in the fault area T_B increased synchronously with stick-slip events and then dropped rapidly. It means that the high temperature caused by stick-slip keeps up only ~20 seconds, which is 20% of that in the jog area. Another observed phenomenon was that the rising process of T_B was different on two faults. Sometimes the rising amplitude of T_B on the right fault was larger than that on the left fault. And at other moments it was the contrary. This means that the two faults of the en echelon structure alternatively come into active, as rising of T_B is primarily associated with the portion of active faulting.

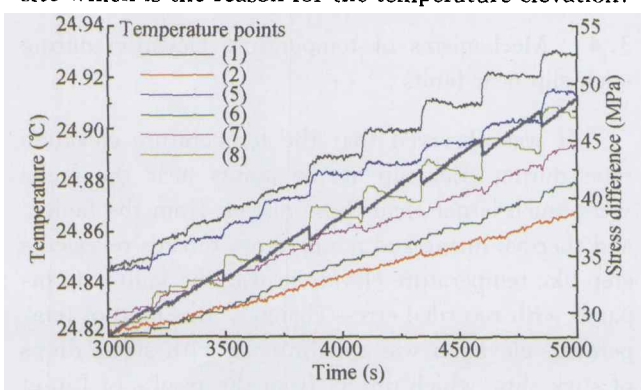

Fig. 4. Variation of temperature at measurement points and differential stress with time in stick slip stage. Gray curve denotes change of stress.

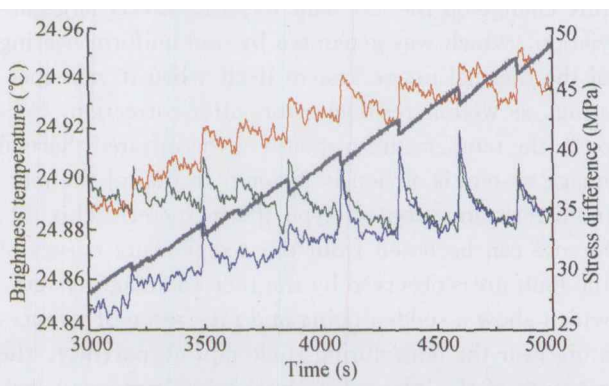

Fig. 5. Variation of brightness temperature of thermal radiation (T_B) in the jog area (red), left fault (green) and right fault (blue) with differential stress (grey).

There are two possible mechanisms for temperature elevation during faulting: strengthened stress and friction. For the first case the amplitude of temperature rising is of small, but with a large thermal amount. The thermal diffusion is slow because the scope concerned by the variation of stress is large. This may be the reason that T_B drops relatively slow after stick-slip in the jog area. In contrast, frictional sliding along fault generates thermal radiation or temperature elevation. Such a process is confined near the fault, producing a relatively small thermal amount which will lose quickly. Thus the temperature near the fault rises considerably in response to a stick-slip event, and after that declines rapidly.

3 Conclusions and discussions

3.1 Similarities and differences of temperature measurements by two kinds of instrumentations

Measurements were made at the same sites by a platinum resistance contact-type thermometer and an infrared thermal system. Comparison of their curves shows a rough consistence. For instance, both are characterized by synchronous temperature elevation produced by stress drop of stick-slip in the jog area and along the faults of the rock sample. The measurements by these two instruments have, however, also distinctive differences. First, for the thermal image system, the temperature fluctuation during the stick-slip process is clearly visible after data correction and filtering, implying that its resolution has been greatly improved with respect to the specified value of the manufacturer. But there are still major residual errors in the measured data of the thermal image system, which makes its temperature resolution is lower than that of the platinum resistance contact-type thermometer. For example, the general trend of temperature change on the left fault has a relatively large deviation, which was generated by non-uniform heating of the thermal image system itself when it was operating, as well as residual errors after correction. Second, the temperature response of the infrared thermal image system is obviously faster than that of the platinum resistance contact-type thermometer. This difference can be noted from the temperature curves of the fault areas observed by the thermal image system, which show a sudden rising and rapid drop of temperature near the fault during stick-slip. Apparently, the response of the infrared thermal image system to such signals is faster than that of the platinum resistance contact-type thermometer.

3.2 Connections of temperature and thermal radiation with stress and strain

In the laboratory, we carried out an experiment of rock deformation and measured variations of the thermal field associated with faulting on the rock specimen. Two apparatuses were used for observations in the test: one measured temperature and the other recorded thermal images on the specimen, from which thermal radiation could be calculated. The experiment was performed under a stable environmental temperature and humidity without atmospheric interference. There was no water and gas involvement in the deformation of the specimen. The measurements of both apparatuses are consistent, demonstrating a relationship between variation of the thermal field with the variation of stress and the stick-slip faulting on the rock specimen.

3.3 Temperature elevation differs at different positions of the faults

Three kinds of temperature elevation were recorded during the experiment. At the points distant from the faults, temperature increases with deformation at a stable and small rate, which reflects the change of the background stress for the entire specimen. At points near the faults, temperature increases in response to stick-slip at a relatively large rate, of which the growth amplitude depends on the distance from the faults. In the jog area the rate of temperature rising was obvious when stick-slip began, implying that fault offset makes the compressive stress of the jog area get large. And in the late stage of deformation, i.e. failure and friction of the jog, temperature rose at a large rate. These phenomena indicated the spatial relationship between the thermal field and stress field during faulting(Fig.6).

3.4 Mechanisms of temperature elevation during stick-slip near faults

It was observed that the temperature elevation rates during stick-slip at the points near the faults were much larger than those distant from the faults, and thermal image and temperature records revealed a step-like temperature elevation near the faults. Compared with recorded stress changes, this kind of temperature elevation was synchronous with stress drops of stick-slip, which differs from the results of Liu et al.[5], who reported that compression generated temperature growth and extension caused temperature de-

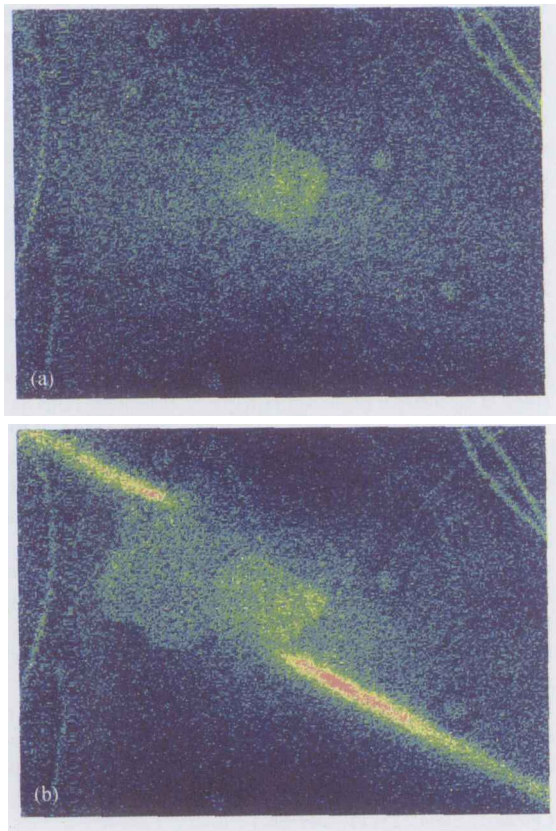

Fig. 6. The thermal images on the central portion of the sample at two moments. (a) shows higher temperature in the jog area by stress concentration. (b) shows higher temperature along faults by frictional sliding and a piece of rock flaked away in the jog area.

cline. Hence, there should be another mechanism underlying this temperature changes. We noted that at most of points near the faults there was a rapid temperature decline for a short time before a sudden temperature elevation, which was particularly prominent at the moment 5791 s when stress dropped. At this moment, the failure and instability of the jog area caused stress drop, making the temperature at points 1, 5, and 6 decline first and then rise. Therefore, it can be concluded that rapid temperature decline is directly related with stress drop and the sudden temperature elevation is associated with the following fast frictional sliding on the faults. It means that change of the deformation mechanism leads to the change of mechanism of temperature elevation.

3.5 A dominant mechanism of temperature elevation in different deformation stages

In the experiment, the sample experienced three deformation stages: elastic deformation, stick-slip sliding, and failure. In the elastic deformation, the temperature rose in the range of 0.01—0.02° mK/s, which was almost the same for all measured points, attributed to stress increasing. When the deformation entered into the stick-slip stage, the rate of temperature elevation at points distant from the faults remained around 0.02° mK/s, a little enlarged; while that near the faults became two times the rate of temperature increasing in the elastic stage, caused by friction on the faults. In the failure stage, the rate of temperature for the areas distant from the faults also changed a little, though having some increase due to the effects of nonlinear growth of stress and surrounding areas of high stress. In contrast, the temperature in the jog area and near the faults was greatly elevated by several magnitudes because of the failure and high speed friction. These analyses demonstrate that the dominant mechanism of deformation changes in different stages, which controls the process of temperature elevation with stress as well as variations of the thermal field.

All of the results may provide a physical basis for analysis of regional tectonic deformation and faulting process including fault instability and dislocation by using satellite thermal image data. In this aspect, there are still many problems to be studied further. For instance, although the experimental results revealed clearly variations of the thermal field caused by stress. The results were recorded in the laboratory where the observation was made in a short distance and with less interference and the data were processed by corrections. In practice satellite data are recorded from a long distance with much interference, so despite the thermal image system may have a much higher resolution. It is still very difficult to analyze temperature rising caused by deformation based on satellite data. Our measured temperature increment is much smaller than the reported temperature anomalies observed prior earthquakes[20], thus, there likely exist other mechanisms induced by stress change. Moreover the relationship between strain rate and heat dissipation rate is also an important issue to be concerned and whether the phenomena found in the laboratory reflects the true in the nature also needs to be proved.

Acknowledgements The authors wish to thank Chen Shunyun, Wang Kaiying and Hu Xiaoyan in our laboratory for their help during the experiment and Gao Xianglin, Shan Xinjian and Qu Chunyan at Institute of Geology China Earthquake Administration for helpful discussions.

References

1 Ma J., Wang Y.P., Chen Sh.Y. et al. Insights into correlation between satellite infrared information and fault activities. Progress in Natural Science, 2006, 15(4): 394—402.

2 Qiang Z.J., Kong L.Ch., Wang G.P. et al. Global atmosphere, thermo-infrared and earthquake activity. Chinese Science Bulletin, 1992, 37(24): 2259—2262.

3 Xu X.D. and Xu X.M. The basic characters and formation mechanism of satellite infrared anomalies before strong earthquakes. Northwestern Seismological Journal, 2001, 23(3): 310—312.

4 Hsieg J. S. Principles of Thermodynamics (in Chinese). Beijing: People's Education Press, 1980.

5 Liu P.X., Chen Sh.Y., Liu L.Q. et al. An experiment on the infrared radiation of surficial rocks during deformation. Seismology and Geology (in Chinese), 2004, 26(3): 502—511.

6 Liu L.Q., Chen G.Q., Liu P.X. et al. Infrared measurement system for rockdeformation experiment. Seismology and Geology (in Chinese), 2004, 26(3): 492—501.

7 Ma J., Du Y.J. and Liu L.Q. The instability of en-echelon cracks and its precursors. J. Phys. Earth, 1986, 34(Suppl): S141—S157.

8 Ma S. L., Deng G.H., Ma W. T. et al. Experimental study on evolution of physical field during deformation of en-echelon faults (1). Seismology and Geology (in Chinese), 1995, 17(4): 327—335.

9 Ma S. L., Deng G.H., Ma W. T. et al. Experimental study on evolution of physical field during deformation of en-echelon faults (2). Seismology and Geology (in Chinese), 1995, 17(4): 336—341.

10 Ma J., Ma S. L., Liu L. Q. et al. Geometrical textures of faults, evolution of physical field and instability characteristics. Acta Seismologica Sinica, 1996, 9(2): 261—269.

11 Cui C.Y., Deng M.D. and Geng N.G. Study on the features of spectrum radiation of rocks under different loading. Chinese Science Bulletin (in Chinese), 1994, 38(6): 538—541.

12 Deng M.D., Geng N.G., Cui C.Y. et al. The study on the variation of thermal state of rocks caused by variation of stress state of rocks. Earthquake Research in China (in Chinese), 1997, 13(2): 179—185.

13 Dong Y. F., Wang L. G., Liu X. F. et al. The experimental research of the infrared radiation in the process of rock deformation. Rock and Soil Mechanics (in Chinese), 2001, 22(2): 134—137.

14 Geng N.G., Cui C.Y., Deng M. D. Remote-sensing observation in the experiment of rock fracture and start of remote-sensing rock mechanics. Acta Seismologica Sinica(in Chinese), 1992, 14(SI): 645—652.

15 Geng N. G. and Cui C. Y. Remote sensing rock mechanics and its application prospects. Progress in Geophysics (in Chinese), 1993, 8(4): 1—7.

16 Wu L.X. and Wang J.Z. Features of infrared thermal image and radiation temperature of coal rocks loaded. Science in China (D) (in Chinese), 1998, 28(1): 41—46.

17 Liu Sh. J., Wu L. X., Wu Y. H. et al. Analysis of affecting factors and mechanics of infrared radiation coming from loaded rocks. Mine Surveying (in Chinese), 2003, 3: 67—70.

18 Qian J. D., Deng M. D., Yin J. Y. et al. A basic experimental study of earthquake prediction in terms of radar technology. Chinese Journal of Sinica (in Chinese), 2005, 48(5): 1103—1109.

19 Yin J.Y., Fang Z. F., Qian J. D. et al. Research on the application of infrared remote sensing in earthquake prediction and its physical mechanism. Earthquake Research in China (in Chinese), 2000, 16(2): 140—148.

20 Ouzounov D. and Freund F. Mid-infrared emission prior to strong earthquakes analyzed by remote sensing data. Advances in Space Research, 2004, 33(3): 268—273.

21 Freund F. Charge generation and propagation in igneous rocks. Journal of Geodynamics, 2002, 33(4—5): 543—570.

22 Wu L. X., Liu S. J., Wu Y. H. et al. Remote sensing-rock mechanics(1)——laws of thermal infrared radiation from fracturing of discontinous jointed faults and its meanings for tectonic earthquake omens. Chinese Journal of Rock Mechanics and Engineering (in Chinese), 2004, 23(1): 24—30.

23 Wu L. X., Liu Sh. J., Wu Y. H. et al. Remote sensing-rock mechanics(2) ——laws of thermal infrared radiation from fracturing of discontinous jointed faults and its meanings for tectonic earthquake omens. Chinese Journal of Rock Mechanics and Engineering (in Chinese), 2004, 23(2): 192—198.

24 Wu L.X., Liu Sh.J., Wu Y.H. et al. Precursors for rock fracturing and failure—Part I: IRR image abnormalities. International Journal of Rock Mechanics & Mining Sciences, 2006, 43: 473—482.